

Extended Cauchy equations of congruent LiNbO₃ in the terahertz band and their applications

GUANG-HAO SHAO, SHI-JUN GE, YUN-CHAO SHI, WEI HU, AND YAN-QING LU*

National Laboratory of Solid State Microstructures, College of Engineering and Applied Sciences, and Collaborative Innovation Center of Advanced Microstructures, Nanjing University, Nanjing 210093, China

*yqlu@nju.edu.cn

Abstract: The refractive indices of ordinary and extraordinary waves (n_o and n_e) of congruent LiNbO₃ (CLN) in the terahertz (THz) band are measured at different temperatures. Extended Cauchy equations are proposed to describe the temperature- and frequency-dependent refractive indices. With less than 0.5% deviation, both n_o and n_e can be obtained accurately. The values of n_o and n_e are ~ 7 and ~ 5.4 , respectively, which are much larger than those in the visible band. The extremely high birefringence (~ 1.6) may lead to some interesting applications of linear, electro-optic, and nonlinear optical effects of CLN. As an example, true zero-order THz waveplates (WPs) could be obtained with considerable low loss based on thin CLN wafers. The working frequency can be tuned by changing the environmental temperature. Moreover, wide bandwidth achromatic THz WPs were also achievable by stacking four CLN wafers together with precise orientation control.

© 2016 Optical Society of America

OCIS codes: (160.3730) Lithium niobate; (260.1440) Birefringence; (110.6795) Terahertz imaging.

References and links

1. M. Tonouchi, "Cutting-edge terahertz technology," *Nat. Photonics* **1**(2), 97–105 (2007).
2. T. Nagatsuma, G. Ducournau, and C. C. Renaud, "Advances in terahertz communications accelerated by photonics," *Nat. Photonics* **10**(6), 371–379 (2016).
3. M. Bass, P. A. Franken, J. F. Ward, and G. Weinreich, "Optical rectification," *Phys. Rev. Lett.* **9**(11), 446–448 (1962).
4. W. Shi, Y. J. J. Ding, N. Fernelius, and K. Vodopyanov, "Efficient, tunable, and coherent 0.18–5.27-THz source based on GaSe crystal," *Opt. Lett.* **27**(16), 1454–1456 (2002).
5. K.-L. Yeh, M. C. Hoffmann, J. Hebling, and K. A. Nelson, "Generation of 10 μ J ultrashort terahertz pulses by optical rectification," *Appl. Phys. Lett.* **90**(17), 171121 (2007).
6. S. Preu, G. H. Döhler, S. Malzer, L. J. Wang, and A. C. Gossard, "Tunable, continuous-wave Terahertz photomixer sources and applications," *J. Appl. Phys.* **109**(6), 061301 (2011).
7. B. Zhang and Y. Gong, "Achromatic terahertz quarter waveplate based on silicon grating," *Opt. Express* **23**(11), 14897–14902 (2015).
8. J.-B. Masson and G. Gallot, "Terahertz achromatic quarter-wave plate," *Opt. Lett.* **31**(2), 265–267 (2006).
9. L. Wang, X.-W. Lin, W. Hu, G.-H. Shao, P. Chen, L.-J. Liang, B.-B. Jin, P.-H. Wu, H. Qian, Y.-N. Lu, X. Liang, Z.-G. Zheng, and Y.-Q. Lu, "Broadband tunable liquid crystal terahertz waveplates driven with porous graphene electrodes," *Light Sci. Appl.* **4**(2), e253 (2015).
10. N. V. Bloch, K. Shemer, A. Shapira, R. Shiloh, I. Juwiler, and A. Arie, "Twisting light by nonlinear photonic crystals," *Phys. Rev. Lett.* **108**(23), 233902 (2012).
11. J. Huo and X. Chen, "Large phase shift via polarization-coupling cascading," *Opt. Express* **20**(12), 13419–13424 (2012).
12. G.-H. Shao, X.-S. Song, F. Xu, and Y.-Q. Lu, "Optical parametric amplification of arbitrarily polarized light in periodically poled LiNbO₃," *Opt. Express* **20**(17), 19343–19348 (2012).
13. Y. Lu, Y. Zhu, Y. Chen, S. Zhu, N. Ming, and Y.-J. Feng, "Optical Properties of an Ionic-Type Phononic crystal," *Science* **284**(5421), 1822–1824 (1999).
14. X. Wu, S. Carbajo, K. Ravi, F. Ahr, G. Cirmi, Y. Zhou, O. D. Mücke, and F. X. Kärtner, "Terahertz generation in lithium niobate driven by Ti:sapphire laser pulses and its limitations," *Opt. Lett.* **39**(18), 5403–5406 (2014).

15. X. Wu, C. Zhou, W. R. Huang, F. Ahr, and F. X. Kärtner, "Temperature dependent refractive index and absorption coefficient of congruent lithium niobate crystals in the terahertz range," *Opt. Express* **23**(23), 29729–29737 (2015).
16. L. Pálfalvi, J. Hebling, J. Kuhl, A. Péter, and K. Polgár, "Temperature dependence of the absorption and refraction of Mg-doped congruent and stoichiometric LiNbO₃ in the THz range," *J. Appl. Phys.* **97**(12), 123505 (2005).
17. J. Kiessling, K. Buse, and I. Breunig, "Temperature-dependent Sellmeier equation for the extraordinary refractive index of 5 mol. % MgO-doped LiNbO₃ in the terahertz range," *J. Opt. Soc. Am. B* **30**(4), 950–952 (2013).
18. X. C. Zhang and J. Z. Xu, *Introduction to THz Wave Photonics* (Springer, New York, 2010), Chap. 3.
19. J. Li and S. T. Wu, "Extended Cauchy equations for the refractive indices of liquid crystals," *J. Appl. Phys.* **95**(3), 896–901 (2004).
20. D. Djukic, G. Cerda-Pons, R. M. Roth, R. M. Osgood, S. Bakhru, and H. Bakhru, "Electro-optically tunable second-harmonic-generation gratings in ion-exfoliated thin films of periodically poled lithium niobate," *Appl. Phys. Lett.* **90**(17), 171116 (2007).
21. G. Poberaj, H. Hu, W. Sohler, and P. Günter, "Lithium niobate on insulator (LNOI) for micro-photonics devices," *Laser Photonics Rev.* **6**(4), 488–503 (2012).
22. G.-H. Shao, Y.-H. Bai, G.-X. Cui, C. Li, X.-B. Qiu, D.-Q. Geng, D. Wu, and Y.-Q. Lu, "Ferroelectric domain inversion and its stability in lithium niobate thin film on insulator with different thicknesses," *AIP Adv.* **6**(7), 075011 (2016).
23. Y.-Q. Lu, Z.-L. Wan, Q. Wang, Y.-X. Xi, and N.-B. Ming, "Electro-optic effect of periodically poled optical superlattice LiNbO₃ and its applications," *Appl. Phys. Lett.* **77**(23), 3719–3721 (2000).
24. Y. Sheng, D. L. Ma, M. L. Ren, W. Q. Chai, Z. Y. Li, K. Koynov, and W. Krolikowski, "Broadband second harmonic generation in one-dimensional randomized nonlinear photonic crystal," *Appl. Phys. Lett.* **99**(3), 031108 (2011).
25. X. Chen, J. Shi, Y. Chen, Y. Zhu, Y. Xia, and Y. Chen, "Electro-optic Solc-type wavelength filter in periodically poled lithium niobate," *Opt. Lett.* **28**(21), 2115–2117 (2003).

1. Introduction

Terahertz (THz) waves, having frequencies between those of microwaves and infrared light, typically are defined as electromagnetic waves in the frequency band of 0.1–10 THz. THz waves are absorbed by water and can penetrate most dielectrics and semiconductors. Thus, they are suitable for various applications in biology and medical sciences, nondestructive evaluation, and quality control [1]. With higher carrier frequencies, THz light is also a promising candidate for high-capacity wireless data transmission [2]. As a result of the increasingly important applications of THz waves, some impressive attempts to generate THz sources have been carried out using difference frequency generation, optical rectification, and photoconductive antennas [3–6]. It is also important to control THz waves with some basic units of THz systems, such as waveplates (WPs), attenuators, routers, and absorbers. Developing methods to tune these devices through external control of environmental conditions will make their use more practicable.

As one class of the basic devices of THz systems, THz WPs have been studied in two configurations. One is the achromatic WP, which promises applicability across a wide frequency band. Achromatic THz quarter-wave plates (QWPs) have been produced using six birefringent quartz plates stacked together or based on a silicon grating [7,8]. Given a $\pm 3\%$ variance of phase retardation, the devices show wideband features. The other configuration is the tunable WP, whose working frequency can be changed by modulating external factors, such as the electric field or temperature. In 2015, Wang et al. proposed tunable liquid crystal terahertz WPs [9]. A THz half-wave plate (HWP) with a thickness of $\sim 250 \mu\text{m}$ can be obtained above 2.1 THz. However, at lower frequencies, such as 1 THz, the thickness of the liquid crystal layer must exceed $500 \mu\text{m}$, which is too thick to fabricate. Therefore, it is necessary for the fabrication of tunable THz WPs to propose a new design based on a suitable material.

Considering the optical counterparts, a simple wafer of birefringence crystal can serve to form THz WPs. Among commonly used optical materials, LiNbO₃, a uniaxial crystal, is known as "the silicon of photonics." In both the visible and near infrared bands, it displays versatile attributes, such as nonlinear properties, electro-optic effects, and piezoelectric

effects [10–13]. It also has been used for generating THz waves [5,14]. Some previous studies have examined the refractive index of stoichiometric LiNbO₃, congruent LiNbO₃ (CLN), and MgO-doped LiNbO₃ [15,16]. When the refractive indices of ordinary and extraordinary waves (n_o and n_e) are measured at several discrete temperatures, the fitting polynomials show temperature independence. Moreover, the studies do not discuss the values of the refractive index at temperatures higher than 30°C. Because the phonon resonance is quite different in the THz band, Sellmeier equations may be invalid, resulting in large deviations between the fitted and measured results [17]. To the best of our knowledge, temperature- and frequency-dependent refractive index equations have not been reported.

In this paper, we first measured n_o and n_e of CLN from 0.5 THz to 1.5 THz at temperatures from 30°C to 130°C with steps of 10°C using a THz time-domain spectrometer (THz-TDS). The results were able to be well fitted by temperature- and frequency-dependent extended Cauchy equations. The result may represent the most accurate refractive index equation of CLN in the THz band because the largest deviation is less than 0.5%. Under normal conditions, n_o is ~ 7 and n_e is ~ 5.4 ; these values are quite impressive. The birefringence of CLN is also very large. Since CLN wafers are easy to polish to designated thicknesses and integrate with other materials, the large values of n_o , n_e , and birefringence may result in many interesting THz applications in the nonlinear and electro-optic regimes. Even a thin wafer of CLN can function well in THz WPs. The working frequency can be easily tuned by adjusting the environmental temperature. Achromatic and temperature-insensitive QWP and HWP also could be obtained based on stacked wafers with bandwidths up to ~ 1.4 THz and ~ 0.9 THz, respectively.

2. Extended Cauchy equations in the THz band

X-cut CLN of 500 μm thickness was used for measuring n_o and n_e simultaneously using the polarization module of a THz-TDS (TAS7500SP; Advantest Corporation, Tokyo, Japan). A THz pulse with a wide frequency range was generated. Then the pulse passed through the CLN sample and interacted with another pulse in the detector for sampling and digitizing. Fourier transform infrared spectroscopy (FTIR) is also an established technique. However, based on current technologies, FTIR spectroscopy usually gives better results with frequencies in excess of 10 THz, while THz-TDS is preferred when the relevant frequencies are below 3 THz [18]. Since the frequency range we studied are among 0.5 THz to 1.5 THz, THz-TDS would be selected. The environmental temperature can be changed by using a homemade temperature controller providing stability of adjustments within $\pm 0.1^\circ\text{C}$. Because the results given by the THz-TDS were the averages of 512 repeated measurements, the effect of temperature variation can be neglected. During our measurements, the temperature changed 100°C in steps of 10°C.

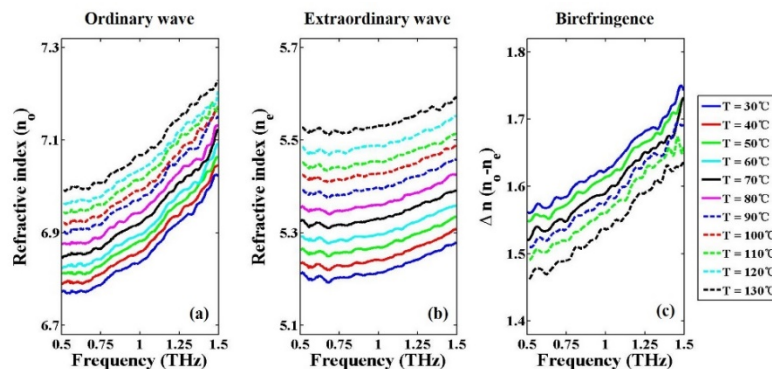


Fig. 1. Values of n_o (a), n_e (b) in the temperature interval of 10°C and values of birefringence (c) in the interval of 20°C over frequencies ranging from 0.5 THz to 1.5 THz.

Figure 1 shows the measured results of n_o and n_e between 0.5 THz and 1.5 THz at 30°C to 130°C in steps of 10°C. From Fig. 1, we see that both n_o and n_e increase at higher frequencies and temperatures. Normally, n_o is ~ 7 while n_e is ~ 5.4 , showing a measure of birefringence of ~ 1.6 , which is quite large. The birefringence is 15 times larger than the value for crystalline quartz, which is impressive. An examination in greater detail shows that n_o changes faster than n_e along with frequency if the temperature remains unchanged. For example, at 30°C, n_o changes from 6.77 to 7.02 while n_e changes from 5.19 to 5.28. However, if the frequency is held constant, n_e increases faster than n_o along with increases in temperature. For instance, at 1 THz, n_o changes from 6.84 to 7.07 while n_e changes from 5.21 to 5.53. The calculated value of Δn , where $\Delta n = n_o - n_e$, thus decreases along with increases in temperature when the frequency is held constant, shown in Fig. 1(c). This relationship also means that Δn can be tuned actively by changing the environmental temperature.

At each of the 11 temperatures in ten-degree steps from 30°C to 130°C, the THz-TDS system measured 131 frequency points. The obtained 1441 data points thus are enough for fitting the dispersion formulas. Usually, in the visible and infrared bands, Sellmeier equations, which contain several terms representing absorption resonances at particular wavelengths, are utilized. However, the phonon resonances are quite different in the THz band. Depicted in Fig. 1, the plots of the refractive indices vary slowly, along with temperature and frequency, without showing abrupt changes. There may be no phonon resonances in the measured THz band. Thus, the Sellmeier equations may be invalid in this range of wavelengths. We also found that CLN performed as a normal, dispersive material in the THz band. Thus, the traditional three-term Cauchy equations may be suitable for fitting n_o and n_e at different temperatures [19]. In this case,

$$n_{e,o}(\nu) \approx A_{e,o} + B_{e,o} \cdot \nu^2 + C_{e,o} \cdot \nu^4, \quad (1)$$

where $A_{e,o}$, $B_{e,o}$, and $C_{e,o}$ are polynomial coefficients. Here, ν stands for frequency in the units of THz. $A_{e,o}$ represents the low frequency limit, which is insensitive to the frequency. $B_{e,o}$ and $C_{e,o}$ are related to the variation trends of n_o and n_e with frequency at different temperatures. The corresponding coefficients at different temperatures are shown in Table 1. We then compared the fitted n_o and n_e with measured ones at 131 frequency points for each sampled temperature. Shown in Table 1, most of the absolute differences between the measured and fitted values are no larger than 0.01, which means that Eq. (1) is quite suitable for temperature-independent refractive index fitting.

A consideration of the counterparts of Sellmeier equations in the visible and infrared bands shows that the fitting equation contains the variates of wavelength and temperature. From this point of view, traditional Cauchy equations must be extended [19]. From Table 1, we see that coefficient $A_{e,o}$ is apparently related to temperature. Thus, $A_{e,o}$ in Eq. (1) can be replaced with a temperature-dependent equation. This paper utilizes $A_{e,o} = A_{1e,o} + A_{2e,o} \cdot T$. Then $A_{1e,o}$ and $A_{2e,o}$ can be deduced from the coefficients of $A_{e,o}$ at different temperatures. Shown in Fig. 1, the trends of changes in both n_o and n_e with frequency are similar at different temperatures. In this condition, updated $B_{e,o}$ and $C_{e,o}$ in the extended Cauchy equations are the averages of the values appearing in Table 1. The new refractive index equation is

$$n_{e,o}(\nu, T) = A_{1e,o} + A_{2e,o} \cdot T + \overline{B_{e,o}} \cdot \nu^2 + \overline{C_{e,o}} \cdot \nu^4, \quad (2)$$

where $A_{1e,o}$, $A_{2e,o}$, $\overline{B_{e,o}}$, and $\overline{C_{e,o}}$ are polynomial coefficients, and $\overline{B_{e,o}}$, and $\overline{C_{e,o}}$ are the average values.

In this case, n_o and n_e are

$$\begin{cases} n_o(\nu, T) = 6.67 + 2.13 \times 10^{-3} T + 9.29 \times 10^{-2} \nu^2 + 15.02 \times 10^{-3} \nu^4 \\ n_e(\nu, T) = 5.10 + 3.17 \times 10^{-3} T - 23.44 \times 10^{-4} \nu^2 + 1.74 \times 10^{-2} \nu^4 \end{cases} \quad (3)$$

where T and ν stand for temperature and frequency with units of Celsius and THz, respectively.

Table 1. Coefficients $A_{e,o}$, $B_{e,o}$, and $C_{e,o}$ of n_o and n_e and deviation between measured and fitted results

Ordinary refractive index (n_o)						
Temperature (°C)	A_o	$B_o (10^{-2} \text{ THz}^{-2})$	$C_o (10^{-3} \text{ THz}^{-4})$	$ n_{\text{fit}} - n_{\text{measure}} $		
				<0.01	0.01 ~0.02	0.02 ~0.03
30	6.74	8.26	20.14	125	6	0
40	6.76	8.52	18.46	127	4	0
50	6.78	8.93	16.87	127	4	0
60	6.80	8.48	19.19	120	11	0
70	6.82	8.93	17.23	121	9	1
80	6.84	9.47	13.71	118	13	0
90	6.87	8.78	18.17	122	9	0
100	6.89	8.97	16.36	129	2	0
110	6.90	10.56	9.19	115	15	1
120	6.92	10.76	6.79	122	9	0
130	6.95	10.57	9.08	119	12	0
Average	—	9.29	15.02	—	—	—
Extraordinary refractive index (n_e)						
Temperature (°C)	A_e	$B_e (10^{-4} \text{ THz}^{-2})$	$C_e (10^{-2} \text{ THz}^{-4})$	$ n_{\text{fit}} - n_{\text{measure}} $		
				<0.01	0.01 ~0.02	0.02 ~0.03
30	5.20	-22.59	1.80	128	3	0
40	5.22	-4.69	1.75	130	1	0
50	5.25	2.13	1.69	129	2	0
60	5.28	-20.80	1.79	131	0	0
70	5.31	-15.66	1.74	128	3	0
80	5.35	-56.39	1.93	130	1	0
90	5.38	-18.88	1.72	129	2	0
100	5.41	-41.65	1.75	130	1	0
110	5.44	-0.21	1.54	129	2	0
120	5.47	-29.81	1.71	129	2	0
130	5.52	-49.31	1.71	131	0	0
Average	—	-23.44	1.74	—	—	—

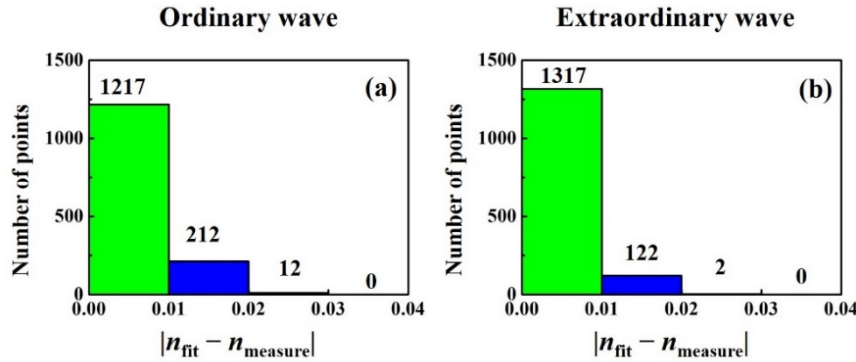


Fig. 2. Absolute value of the deviation between measured n_o (a) and n_e (b) and the fitted values using extended Cauchy equations for $131 \times 11 = 1441$ data points.

Figure 2 shows the absolute values of deviation between measured n_o/n_e and the fitted values using the expressions in Eq. (3), that is, the extended Cauchy equations. Most of the deviations of the fitted values are less than 0.01. The largest errors of n_o and n_e are 0.0253 and 0.0216, respectively. The fitting in our work was more successful than results presented in previous reports [17]. Even in the less successful cases, the error of the fitting was lower than 0.5%. To the best of our knowledge, these results are the most accurate temperature- and frequency-dependent refractive index equations. The extended Cauchy equations can be used to calculate both n_o and n_e at specific temperatures and frequencies from 30°C to 130°C in the band from 0.5 THz to 1.5 THz.

3. CLN as a tunable THz WP

Based on the extended Cauchy equations, Δn can vary from 1.57 to 1.46, 1.64 to 1.53, and 1.75 to 1.64 at 0.5 THz, 1.0 THz, and 1.5 THz, respectively. Normally, Δn decreases by 0.11 with a temperature increase of 100°C. For the p th-order QWP, the thickness of the sample, d_{QWP} , can be deduced from $\Delta n \times d_{\text{QWP}} = (4p + 1) \times \lambda / 4$. In the case of an HWP, the thickness of the sample, d_{HWP} , follows from the relation $\Delta n \times d_{\text{HWP}} = (2p + 1) \times \lambda / 2$. If a 45°-polarized THz wave transmits through a 500 μm CLN, the polarization states will be changed. Some suitable frequencies for QWP and HWP can be calculated at 30°C and 130°C using the extended Cauchy equations, as shown Table 2 and marked by K_1 to K_4 in Fig. 3(a).

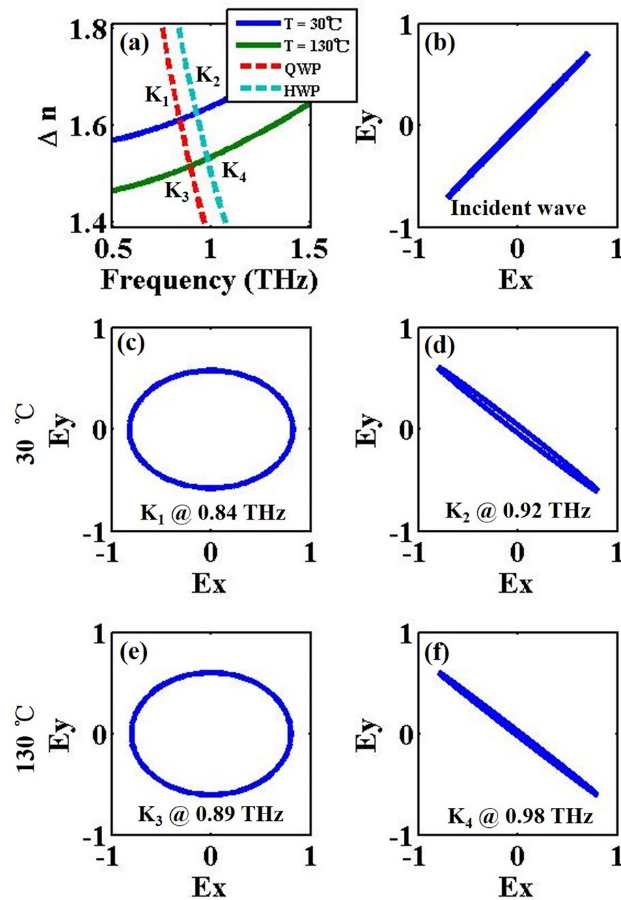


Fig. 3. Determination of suitable frequencies for QWP and HWP. (a) K_1 , K_2 , K_3 , and K_4 represent the corresponding frequencies of QWP and HWP at 30°C and 130°C based on the extended Cauchy equations. The polarization states of (b) the incident wave, (c) 30°C at 0.84 THz, (d) 30°C at 0.92 THz, (e) 130°C at 0.89 THz, and (f) 130°C at 0.98 THz, respectively.

Table 2. Calculated frequencies for QWP and HWP at 30°C and 130°C

Temperature	QWP	HWP
30°C	0.84 THz	0.92 THz
130°C	0.89 THz	0.98 THz

The polarization states of corresponding frequencies and temperatures are shown in Figs. 3(c)–3(f). The working frequency changes by 0.05 THz with a 100°C temperature difference. The results demonstrate that X-cut CLN wafers can work effectively as tunable QWPs and HWPs. Moreover, they indicate that our extended Cauchy equation can accurately describe the refractive indices of CLN.

The birefringence of CLN is quite large. Thus, a very thin wafer of CLN can serve as a QWP or HWP. When the frequency is 1 THz, for example, the CLN wafer can be as thin as ~47 μm and ~94 μm for QWPs and HWPs, respectively. These configurations may have some integrated applications. Even though the absorption coefficient is relatively large [15], the transmission efficiency is still considerable because a true zero-order WP is quite thin. Figures 4(a), 4(b), 4(d), and 4(e) show the transmission efficiencies for true zero-order QWPs and HWPs in the directions of ordinary and extraordinary waves if only absorption loss is considered. At higher temperatures, the efficiency may decrease a little. Assessments of

absorption losses at 130°C indicate that efficiencies are greater than 64% and 41% for QWP and HWP, respectively. These measures compare favorably to results for WPs using crystalline quartz. The conventional Fresnel reflection equation is probably invalid if the film thickness is far smaller than the wavelength, while further experimental verification is still required. Since the thicknesses of true zero-order WPs are still comparable with THz wavelengths in the sample. The Fresnel reflection equations may still be able to predict the reflection loss with fair accuracy.

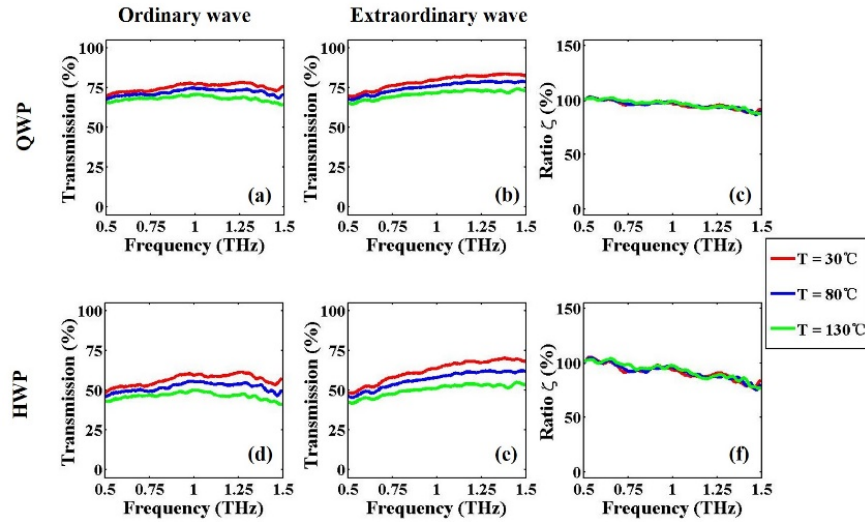


Fig. 4. Transmission efficiencies for true zero-order QWPs and HWPs at different temperatures. (a) QWP transmission efficiency in the direction of ordinary waves. (b) QWP transmission efficiency in the direction of extraordinary waves. (c) True zero-order QWP transmission ratio ζ . (d) HWP transmission efficiency in the direction of ordinary waves. (e) HWP transmission efficiency in the direction of extraordinary waves. (f) True zero-order HWP transmission ratio ζ .

We found that the transmitted waves were not perfectly circular-polarized in the circumstances depicted in Figs. 3(c) and 3(e) and not perfectly -45° -linear-polarized in the results depicted in Figs. 3(d) and 3(f). These outcomes may result from different absorption coefficients and reflection losses in different transmission efficiencies in the directions of ordinary and extraordinary waves. They also might be resolved if true zero-order WPs were used. We defined the transmission ratio ζ to be the ratio of the transmission efficiency of the ordinary wave to the transmission efficiency of the extraordinary wave. For examples of true zero-order QWP and HWP, ζ varies in acceptable ranges from 87% to 103% and 75% to 105%, respectively. Shown in Figs. 4(c) and 4(f), ζ is close to 100% at lower frequencies, indicating the CLN may be more suitable for low-frequency WPs. Reflection losses can be decreased efficiently if anti-reflection layers are deposited on both surfaces of the sample, just as in the visible and infrared bands.

4. Discussions

This paper presents, for the first time, extended Cauchy equations for both n_o and n_e . Calculating the thickness of QWP and HWP based on CLN offers a convenient approach. State-of-the-art techniques employing the Czochralski method and polishing can yield X-cut CLN wafers 2 mm to 30 μm thick. Thinner wafers can be fabricated using crystal-ion slicing. Production of a 10- μm -thick sample was demonstrated [20]. Even submicron-thick CLN thin films have been commercialized and studied [21,22]. Thus, WP based on CLN can be used for all THz bands in the frequency range from 0.1 THz to 10 THz. Moreover, even when

temperature controllers are not in use, changing external electric fields can also serve as effective way to tune the refractive index and determine the center frequency of WP [23]. Another kind of tunable THz WP thus can be obtained by applying voltages through graphene electrodes.

Because CLN is quite sensitive to environmental temperatures, the center wavelength of the proposed WP can be easily tuned. However, in some other situations, achromatic WPs are preferred as previously mentioned. Masson and Gallot proposed a design by stacking six quartz plates together at different angles [8]. Therefore it is also desired to develop achromatic QWPs and HWPs based on CLN in the THz band. Here two constraints are employed in the calculation. Firstly, dephasing of 3% for QWP and 5% for HWP are the limits for achromatic QWP and HWP [7,8]. Secondly, the wavelength should be within 0.5 – 2.5 THz to ensure accurate extended Cauchy coefficients. By using genetic algorithm, we obtained optimized designs for achromatic WPs with only four CLN plates. The corresponding parameters are shown in Table 3.

Table 3. Calculated thicknesses and orientations for four wafer stacking QWP and HWP

Calculated thicknesses and orientations for four wafer stacking QWP				
	1	2	3	4
Thickness (μm)	219	151	401	279
Angle (deg)	50.4	8.0	33.1	147.5
Calculated thicknesses and orientations for four wafer stacking HWP				
	1	2	3	4
Thickness (μm)	411	354	392	42
Angle (deg)	84.0	26.0	79.1	120.7

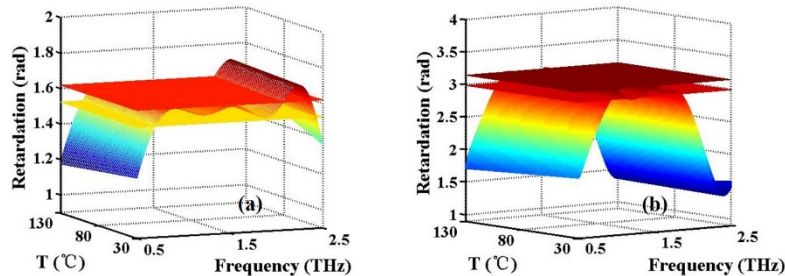


Fig. 5. Phase retardation versus temperature and frequency of achromatic QWP (a) and HWP (b). Inserting plates in the figure indicate the dephasing constraints of 3% for QWP (a) and 5% for HWP (b), respectively.

Table 4. Comparison of achromatic WPs between previous designs and ours.

Type	QWP	QWP	QWP	HWP
Material	Silicon	Quartz	LiNbO ₃	LiNbO ₃
Center frequency	1 THz ¹	1 THz	1.4 THz	1.4 THz
Bandwidth	0.45 THz	1.4 THz	~1.4 THz	~0.9 THz
Temperature dependence	Not mentioned	Not mentioned	Independent	Independent
Thickness	1 mm	31.45 mm	1.05 mm	1.2 mm
Fabrication processes	Photolithography and deep reactive ion etching	Six plates stacked with different angles	Four plates stacked with different angles	Four plates stacked with different angles
References	[7]	[8]	Our work	Our work

¹ The center frequency could be changed with different designs. Here, 1 THz is selected as an example.

Figure 5 shows the phase retardation versus temperature and frequency. If the temperature changes from 30°C to 130°C, the bandwidth varies from 1.37 THz to 1.40 THz for QWP while varies from 0.91 THz to 0.94 THz for HWP, indicating such devices are almost temperature insensitive. Table 4 compares previous proposals for WPs with our designs. It could be found that our design is compact and easy to fabricate, while with considerable wide bandwidth.

Note that, LiNbO₃ is famous for demonstrating nonlinear and electro-optic properties in the visible and infrared bands. In particular, by employing quasi-phase matching, periodically poled LiNbO₃ can achieve effective nonlinear frequency conversion and polarization rotation [24,25]. At this point, however, few studies have focused on such topics in the THz band. The extended Cauchy equations can provide good references for designing domain structures. Rough estimates of the coherent length for second harmonic generation and polarization rotation at 1 THz are ~3 mm and ~100 μm, respectively. This structure can be fabricated easily using current techniques.

5. Conclusion

We make the first presentation of extended Cauchy equations for CLN, showing both frequency and temperature dependence. The equation shows a deviation of less than 0.5%, thus providing a reliable reference for CLN-related THz studies. Under normal conditions, n_o is ~7, n_e is ~5.4, and Δn is ~1.6. These results are quite impressive. Such large refractive indices may yield some interesting applications in the nonlinear and electro-optic regimes. Also, a thin wafer of CLN can work in temperature-tunable THz WPs. The transmission efficiencies of true zero-order QWPs and HWPs are higher than 64% and 41%, respectively. These measures of performance are comparable to those obtained for crystalline quartz. Also, four thin CLN wafers stacks with designed orientation could realize achromatic WPs with wide bandwidth. Our results give good references for THz related studies, showing potential applications in the future

Funding

National Natural Science Foundation of China (Grants No. 61490714, 61225026 and 11604144); Program for Changjiang Scholars and Innovative Research Team at the University (IRT13021).

Acknowledgments

The authors thank Dr. Ya-ping Ruan for his kind help in making the temperature controller.